Journal of ELECTRONIC MATERIALS, Vol. 41, No. 10, 2012
DOI: 10.1007/s11664-012-2113-7
© 2012 TMS

MBE Growth of MCT on GaAs Substrates at AIM

J. WENISCH,[1,2] D. EICH,[1] H. LUTZ,[1] T. SCHALLENBERG,[1] R. WOLLRAB,[1] and J. ZIEGLER[1]

1.—AIM INFRAROT-MODULE GmbH, Theresienstrasse 2, 74072 Heilbronn, Germany. 2.—e-mail: jan.wenisch@aim-ir.com

Driven by the need for more efficient and cost-effective production of infrared (IR) detectors as well as the demands for novel (third-generation) device concepts, a large amount of effort has been spent on the development of molecular beam epitaxy (MBE) for fabrication of high-quality HgCdTe (MCT) layers on both CdZnTe and alternative substrates. The bulk of recent publications focuses on Si as an alternative substrate material. The intent of this paper is to highlight the potential benefit of using GaAs as an alternative substrate material by presenting MCT material grown by MBE on GaAs at AIM. Mid-wave IR MCT/GaAs material has been processed by AIM's standard planar *n*-on-*p* technique. Focal-plane arrays with 640×512 pixels and a 15 μm pitch design show low and homogeneous noise equivalent temperature difference of 18.3 ± 2.0 mK at 99.31% operability. To analyze the feasibility of MBE growth of long-wave IR MCT on GaAs, a layer with 8.8 μm cutoff at 80 K has been fabricated and processed into 640×512 pixels, 15-μm-pitch arrays. Initial current–voltage characterization yields promising results and illustrates the potential of MBE growth for LWIR MCT detector production.

Key words: Infrared detectors, HgCdTe, MBE, GaAs substrates

INTRODUCTION

For decades, liquid-phase epitaxy (LPE) has been the fabrication method of choice for production of MCT infrared (IR) detectors. However, several developments in the IR market have driven LPE technology to the limit of its capability. First, the industry has to satisfy the increasing demand for low-cost, high-performance detectors, a task for which LPE is ill equipped. The problem is rooted in the fact that MCT growth by LPE has only ever been successful on the lattice-matched CdZnTe substrate. While AIM has the capability to produce these substrates in-house, eliminating the need for a commercial supplier, the price of these substrates is still very high. Additionally, they are only available in relatively small sizes and are difficult to handle due to their brittle nature. The second limit of LPE technology is related to the demand for expanded detector functionality such as the ability to detect two wavelengths in a single MCT "dual-band" detector pixel. Such devices are commonly referred to as third-generation detectors. As LPE is a process where the crystal is grown from liquid melt, it is not feasible to vary the composition of a layer during growth, or introduce doping profiles, as would be required for multiband detection.

A technology which has the potential to overcome the limitations of LPE is molecular beam epitaxy (MBE). In contrast to LPE, the constituent elements are provided in the form of directed molecular beams in an ultrahigh-vacuum (UHV) environment. Since the intensity and therefore the flux ratio of the beams can be varied during growth, multilayered MCT structures become possible. Better material homogeneities over large wafer areas compared with LPE are also expected. Another major benefit of MBE is the availability of alternative substrates which can replace CdZnTe. High-quality alternative substrates are commercially available from a number of suppliers at a fraction of the cost of CdZnTe. As these substrates can be fabricated to a size of up to several inches in

(Received October 20, 2011; accepted April 19, 2012; published online May 9, 2012)

diameter, postepitaxial processes also benefit from the ease of processing one large wafer as opposed to several small ones. All these factors work together to reduce the production cost of MCT IR detectors.

There are three obvious candidates as alternative substrates to replace CdZnTe, namely Si,[1,2] Ge,[3] and GaAs.[2,4] All three share a very large lattice mismatch of 19.0% (Si) or 14.3% (Ge and GaAs) to MCT. This fact is the root of one of the biggest challenges that MBE growth of MCT on alternative substrates has to overcome. The interface region between substrate and the following II–VI material is the source of a large number of threading dislocations.[5] These dislocations can extend vertically through the entire layer stack and may act as alternative current paths which degrade the diode performance of affected detector pixels. InSb has received some attention as an alternative substrate material due to its near-perfect lattice match to LWIR MCT. While this property would avoid the problem of threading dislocation generation, problems with the low thermal stability leading to In diffusion and the poor IR transmission of InSb have so far prevented its successful use in device fabrication.[6]

There are a number of arguments for or against each of these substrates, but to date, no clear favorite has been determined. AIM has chosen GaAs substrates with crystal orientation of (211) for the development of its MBE on alternative substrates activities. One benefit of GaAs is its "epiready" availability. The oxide layer can easily be removed thermally, rendering any pregrowth treatment of the wafers unnecessary. A second benefit originates from the binary nature of the GaAs crystal. Where MCT layers on Si or Ge require a ZnTe/CdTe buffer layer to ensure growth in the (211) crystal orientation, MCT will grow in this orientation on GaAs without requiring a ZnTe layer.

MBE EQUIPMENT

To pursue its MBE activities, AIM installed a Veeco Gen20A MBE system in 2009, which has recently been upgraded to dual growth chamber configuration. The system consists of a central cluster module which houses the automated transfer system and acts as a hub to all other connected modules. Attached to the cluster module are a load lock, a storage module, a preparation chamber, as well as the two growth chambers. Each growth chamber is equipped with 12 effusion cell ports, a reflection high-energy electron diffraction (RHEED) system, and retractable beam flux monitor. The system is customized for the special demands of mercury growth. Excess mercury can be removed from the growth chambers via two connected mercury reclamation modules. Each reclamation module houses a 3000 L/s cryopump to maintain UHV in the growth chamber. Although both growth modules are designed identically, their use is separated into alternative-substrate MCT growth (the focus of this paper) and MCT layer growth for dual-band detector production. The system is capable of handling wafers up to a diameter of 4 inches. Hg, Te, and CdTe are evaporated from valved effusion sources which enable fast flux variations and provide excellent run-to-run stability.

As no pregrowth treatment of the epiready GaAs wafers is necessary, the MBE process commences with an oxide desorption step in the preparation chamber at 810°C heater temperature under As_4 flux. Following this step, the wafer is transferred into the growth chamber, where a 1-μm-thick CdTe buffer is deposited at about 315°C at growth rate of 1 μm/h. After buffer growth, the wafer is cooled to about 180°C and MCT growth begins at growth rate of ~2 μm/h. For growth development purposes, most MCT layers were 5 μm thick on top of a 1-μm CdTe buffer layer.

MBE MATERIAL QUALITY

The quality of the MBE-grown material was extensively monitored during the process of initial development. Over the course of the first campaign, the CdTe buffer growth was established. At growth temperature of about 315°C, a typical growth rate of 1 μm/h was obtained. The layers generally show a low density of macrodefects larger than 10 μm on the order of 4 cm^{-2}. The origin of these defects is suspected to be surface contamination of the wafer caused by handling steps before the growth process. The layer thickness is very homogeneous with variation of less than ±0.4% over the whole wafer for a 5-μm-thick layer. For a layer of similar thickness, rocking curve full-width at half-maximum (FWHM) of ~80 arcsec could be measured by high-resolution x-ray diffraction (HRXRD) with a four-crystal monochromator.

In contrast to the CdTe material, which is rather insensitive to nonoptimal growth conditions, MCT layers react to deviations as low as ±2°C from the optimal growth temperature with significantly higher defect formation. This extremely small growth window requires extensive process optimization. In the current stage of development at AIM, defect densities of 50 cm^{-2} in the 4 μm to 10 μm bin and 4 cm^{-2} for the >10 μm bin have been achieved. HRXRD rocking curves with FWHM of ~60 arcsec document the good crystal quality of the MCT layers.

The composition homogeneity of the material is reflected in its cutoff wavelength, which can be measured by Fourier-transform infrared spectroscopy (FTIR). Figure 1 shows a FTIR scan across 8 cm of the wafer, measuring 17 points along the diameter. The wafer has an average cutoff at 300 K of 4.53 μm. The center of the wafer out to ±20 mm is very homogeneous with variation of less than 0.66%. Farther out towards the edge, the cutoff drops by a maximum value of 0.11 μm (−2.4%). This inhomogeneity is attributed to a nonoptimized flux

profile from the CdTe or Te effusion cells. Further optimization of the cells is expected to reduce or eliminate the remaining inhomogeneity.

As mentioned earlier, the large lattice mismatch between substrate and MCT causes a large number of threading dislocations to nucleate in the interface region. The points of emergence of these threading dislocations at the MCT surface are quantified by etch pit density (EPD) analysis using the Schaake etch.[7,8] The best EPD that has been measured on AIM MCT layers is 1.5×10^7 cm^{-2}. The best EPD values that have been reported for MCT on alternative substrates are in the low 10^6 cm^{-2} region.[9] To achieve these literature values, a number of techniques such as *in situ*[10] and *ex situ*[11] cyclic annealing or lattice-matched buffers were utilized, none of which have been implemented at AIM yet.

To investigate how the material is distributed along the growth axis, secondary-ion mass spectroscopy (SIMS) analysis has been performed. The measured sample consisted of a 7.2-μm-thick MCT layer on a 1.0-μm CdTe buffer on GaAs. As the plot in Fig. 2 shows, the material is distributed homogeneously throughout the depth of the layers. The surface was not passivated, which is reflected in the change of oxygen and Hg counts at the left end of the plot. An important observation is the extent of the Ga diffusion into the first 200 nm to 300 nm of the buffer layer, which proves that there is no unintentional Ga doping of the MCT layer.

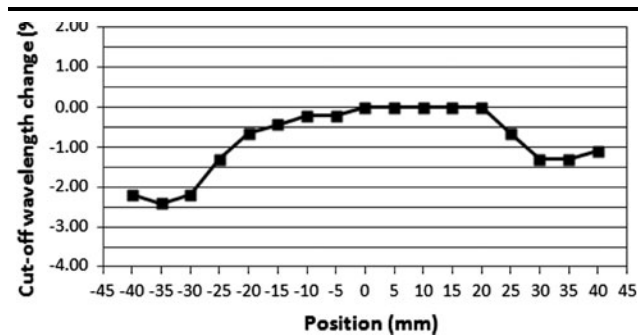

Fig. 1. FTIR scan of the MCT cutoff wavelength across 17 points along the diameter of a MCT/GaAs wafer. Average cutoff at 300 K is 4.53 μm with maximum variation of 0.11 μm (2.4%).

MWIR MCT FPA PERFORMANCE

The first evaluation of focal-plane array (FPA) performance of MBE-grown material was performed on a MCT/CdTe/GaAs wafer which was processed into 60 arrays of 640×512 pixels with 15 μm pitch size by AIM's standard planar *n*-on-*p* technique. The detector chips were then hybridized to the readout integrated circuit (ROIC) and integrated into a standard integrated detector cooler assembly (IDCA). Electrooptical measurements were performed at a detector temperature of 80 K at which the cutoff wavelength was 5.29 μm. The integration time was 7.25 ms at half well filling of the integration capacitor. An *F*# of 4.6 was used. Under these conditions a low mean noise equivalent temperature difference (NETD) of 18.3 mK with standard deviation of 2.0 mK was obtained. As both the NETD histogram (Fig. 3a) and the NETD pixel map (Fig. 3b) indicate, the NETD is distributed very homogeneously over the whole array. The operability of the array is 99.31%, with an operable pixel being defined as having an NETD value between 0 mK and twice the $\mathrm{NETD}_{\mathrm{mean}}$. In the defective pixel map shown in Fig. 3c, several clusters of defective pixels are present. All of the large clusters can be traced to void defects that overlap with the area of several pixels. The material which was used to fabricate this array originates from an early stage of growth development, where macrovoids and

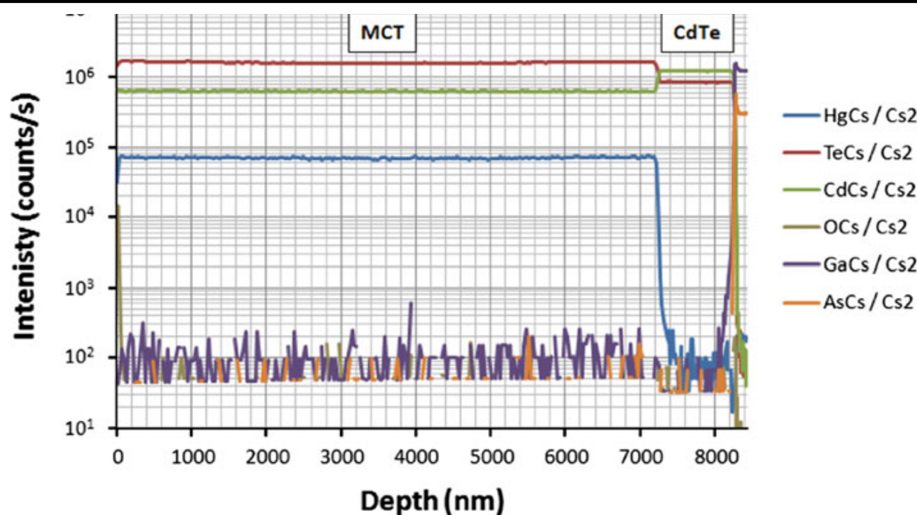

Fig. 2. SIMS depth profile of a MCT/CdTe/GaAs sample. Layer thickness is 7.2 μm for MCT and 1.0 μm for CdTe buffer. The material is distributed homogeneously throughout the depth of the layers. Ga diffusion from the substrate stops well inside the buffer layer.

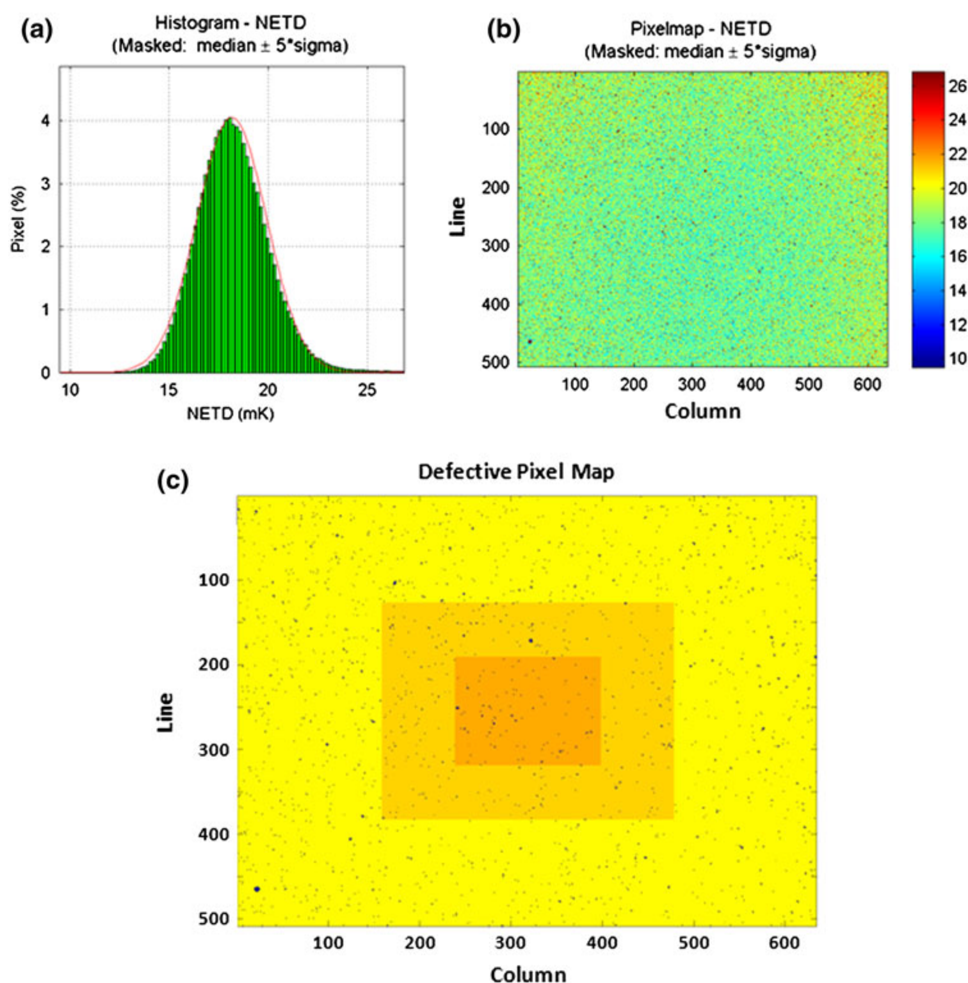

Fig. 3. Electrooptical measurements on a 5.29-μm-cutoff MBE MCT/GaAs FPA at 80 K. The NETD histogram (a) and NETD pixel map (b) show the very homogeneous distribution of the NETD of 18.3 $\pm$ 2.0 mK. A defective pixel map (c) of the array shows 0.69% defective pixels. A pixel is defined as defective if its NETD lies outside [0,2] $\times$ $NETD_{mean}$.

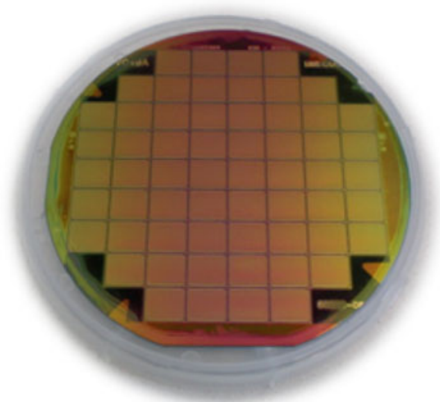

Fig. 4. LWIR MCT on (211) GaAs substrate with 100 mm diameter. The wafer has been processed by AIM's standard planar technique into 60 arrays of 640 $\times$ 512 pixels with 15 μm pitch size.

high-temperature voids were a lot more prevalent than in layers grown with the most recent set of optimized growth parameters.

LWIR MCT MATERIAL

To evaluate the feasibility of applying MBE growth on GaAs substrates to the fabrication of LWIR MCT material, a layer with cutoff of 5.88 μm at 300 K was grown. No adaption of process parameters from standard MWIR material growth was performed for the altered material composition. Analogous to the MWIR detector, the LWIR wafer was processed by standard planar n-on-p technique, with vacancy doping for the p-type region, into 60 arrays of 640 $\times$ 512 pixels with 15 μm pitch size. Figure 4 shows a picture of the wafer at the stage of the first electrical measurements. Six representative arrays out of the 60 were chosen from across the wafer for test diode characterization. The test diode area was 50 μm $\times$ 57 μm. The arrays were cooled to a temperature of 80 K at which all arrays displayed a cutoff wavelength of 8.8 μm to 8.9 μm. The measurements were performed at background temperature of 300 K. In Fig. 5, all 12 diode characteristics are plotted as a set of curves. For all diodes, a maximum dynamic resistance of higher than

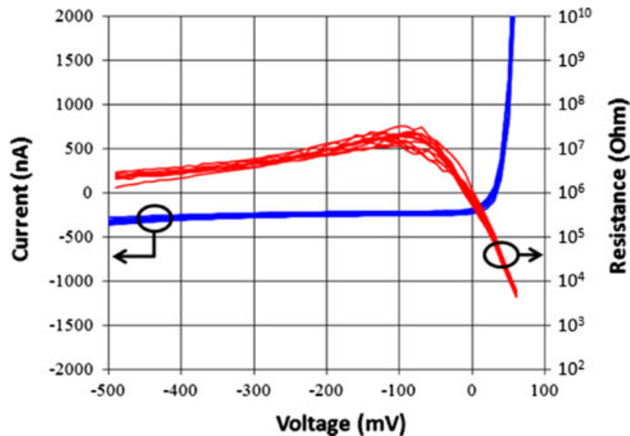

Fig. 5. Diode characteristics of 12 test diodes from six arrays on a LWIR MCT/GaAs MBE wafer. Cutoff wavelength for all diodes is 8.8 μm to 8.9 μm at 80 K. The diode current and dynamic resistance are plotted as a function of the applied bias voltage. Background temperature is 300 K.

1×10^7 Ω could be achieved. The current at reverse bias shows a pronounced flat plateau out to the highest applied bias voltage of -500 mV. Considering the early stage of growth development at which this wafer was produced and especially the fact that no dedicated efforts were undertaken to reduce dislocation density, this result is very encouraging. A full electrooptical FPA characterization will be performed in the near future.

CONCLUSIONS

MBE technology in general is necessary for production of advanced third-generation IR detectors. Alternative substrates are a key component for cost reduction. AIM has chosen to focus on (211) GaAs and has established the growth of MCT layers on CdTe buffers on this substrate. The work is being performed in a Veeco Gen20A dual growth chamber MBE system, which is specifically designed to deal with the demands of mercury growth. In the current stage of growth development, very good material quality with good homogeneity has been achieved. Good FPA performance of MWIR MCT/GaAs material has been demonstrated with a 640×512 pixels, 15-μm-pitch detector. An identical design was used to evaluate the potential of MBE MCT/GaAs for LWIR detector production. Diode characteristics from several arrays of a LWIR MCT wafer show very promising results and warrant further investigation of LWIR MBE growth on GaAs substrates.

REFERENCES

1. M. Carmody, J.G. Pasko, D. Edwall, E. Piquette, M. Kangas, S. Freeman, J. Arias, R. Jacobs, W. Mason, A. Stoltz, Y. Chen, and N.K. Dhar, *J. Electron. Mater.* 37, 1184 (2008).
2. L. He, X. Fu, Q. Wei, W. Wang, L. Chen, Y. Wu, X. Hu, J. Yang, Q. Zhang, R. Ding, X. Chen, and W. Lu, *J. Electron. Mater.* 37, 1189 (2008).
3. J.P. Zanatta, G. Badano, P. Ballet, C. Largeron, J. Baylet, O. Gravrand, J. Rothman, P. Castelein, J.P. Chamonal, A. Million, G. Destefanis, S. Mibord, E. Brochier, and P. Costa, *J. Electron. Mater.* 35, 1231 (2006).
4. C.D. Maxey, J.C. Fitzmaurice, H.W. Lau, L.G. Hipwood, C.S. Shaw, C.L. Jones, and P. Capper, *J. Electron. Mater.* 35, 1275 (2006).
5. R. Beanland, D.J. Dunstan, and P.J. Goodhew, *Adv. Phys.* 45, 87 (1996).
6. T.J. De Lyon, R.D. Rajavel, B.Z. Nosho, S. Terterian, M.L. Beliciu, P.R. Patterson, D.T. Chang, M.F. Boag-O'Brien, B.T. Holden, R.N. Jacobs, and J.D. Benson, *J. Electron. Mater.* 39, 1058 (2010).
7. H.F. Schaake and A.J. Lewis, *Mater. Res. Soc. Symp. Proc.* 14, 301 (1983).
8. J.R. Yang, X.L. Cao, Y.F. Wei, and L. He, *J. Electron. Mater.* 37, 1241 (2008).
9. J.D. Benson, R.N. Jacobs, J.K. Markunas, M. Jamie-Vasquez, P.J. Smith, L.A. Almeida, M. Martinka, M.F. Vilela, and U. Lee, *J. Electron. Mater.* 37, 1231 (2008).
10. Y. Chen, S. Farrell, G. Brill, P. Wijewarnasuriya, and N. Dhar, *J. Cryst. Growth* 310, 5303 (2008).
11. G. Brill, S. Farrell, Y.P. Chen, P.S. Wijewarnasuriya, M.V. Rao, J.D. Benson, and N. Dhar, *J. Electron. Mater.* 39, 967 (2010).